International Journal of
Plasma Environmental Science and Technology

Regular Paper

DOI: 10.34343/ijpest.2020.14.e01004

Plasma candle: A new type of scaled−up plasma jet device

Hyun-Ha Kim[1, *], Nozomi Takeuchi[2], Yoshiyuki Teramoto[1], Atsushi Ogata[1], Ayman A. Abdelaziz[1, 3]

[1]Department of Environmental Management Technology, National Institute of Advanced Industrial Science and Technology (AIST), 16−1 Onogawa, Tsukuba, Ibaraki 305−8569, Japan

[2]Department of Electrical and Electronic Engineering, Tokyo Institute of Technology, 2−12−1 Ookayama, Tokyo 152−8552, Japan

[3]Physics Department, Assiut University, Assiut 71516, Egypt

* Corresponding author: hyun-ha.kim@aist.go.jp (Hyun-Ha Kim)

Received: 31 January 2020
Revised: 2 March 2020
Accepted: 5 March 2020
Published online: 7 March 2020

Abstract

This paper presents a new type of plasma jet device that incorporates porous ceramic plate perpendicular to the helium gas flow. This new configuration enables a plasma jet with a nozzle diameter larger of 10 mm – 31 mm, which has not previously been reported for a plasma jet. We call this large-diameter plasma jet a plasma candle. The advantage of this new device is that a treating area can be extended up to 100 ~ 754 mm^2. The pore size of the ceramic was found to be important to form a stable plasma candle. The optimum pore size was found to be approximately10 μm. The imaging of the plasma jet revealed that charge build-up on the downstream of the porous ceramic plate and its growth toward the nozzle outlet is an important aspect in the scale up of plasma jet.

Keywords: Plasma candle, plasma jet, porous ceramic plate, scale up.

1. Introduction

A plasma jet is a type of atmospheric pressure nonthermal plasma in which the plasma afterglow (plume, bullet, or stream) is extended from the tip of the nozzle [1, 2]. Atmospheric pressure plasma jets (APPJ) offers attractive tool for a wide variety of applications. Inert working gases (typically helium, argon, or a mixture of the two) are used to form stable plasma jets. One of important roles of inert working gases is the formation of stable glow-like discharges under atmospheric pressure. The high energy level of inert gases enables strong Penning ionization which is essential for the propagation plasma plume from a nozzle toward targets at a distance up to 10 cm [3]. Another important role is played by the larger diffusion coefficients of reactive species in inert gases when compared with in air. For example, the diffusion coefficient of OH in He (0.87 cm^2 s^{-1}) is approximately four times larger than that in the air (0.21 cm^2 s^{-1}) under the typical operating conditions of APPJ (i.e., under atmospheric pressure and ambient temperature). In the last decade, APPJs have been the subject of intensive research both in fundamental study of physicochemical properties [1] and in the development of various applications such as surface modification, bacterial inactivation [4], and medical treatment [5−7]. The diagnostics of reactive species and gas flow patterns (laminar vs. turbulent) have been investigated using laser-induced fluorescence (LIF) [8], Schlieren imaging [9, 10], and fast imaging using an intensified charge coupled device (ICCD) camera [11]. The upper limit of the inner diameter of APPJs seems to be approximately 8 mm [12] and typical nozzle size is found in the range of 2 – 6 mm. Downsizing of the jet diameter has been managed successfully in the range of 100 – 500 μm [13−15] and the smallest nozzle size even extends down to 100 nm [16]. The small nozzle size commonly used (a few millimeters in inner diameter) leads to a limited treatment area of 5 – 30 mm^2. To overcome this limitation, bundle arrays of multiple nozzles have been developed. For example, Nie *et al*. [17] and Kim *et al*. [18] reported bundle arrays of 7 nozzles for treatment of large-area surfaces. Another example is a linear-array of 10 – 21 nozzles [19−21]. Lietz *et al*.

compared experiments and two-dimensional modeling of linear multi-jet device [22]. In the case of both bundle and linear arrays, uniformity of the plasma jet in between the nozzles cannot be obtained and scanning of the jet array or substrate is necessary. Dobrynin and Fridman reported 2D "plasma bullets concept" based on the planar dielectric-barrier discharge energized with a pulsed power supply [23]. Despite tremendous advances in the understanding and the widespread use of plasma jet, scale up of nozzle itself has received relatively less attention and requires further studies.

In this work, we report a new type of plasma jet reactor that can extend the size of nozzle inner diameter up to 20 mm and is capable of treating an area of 314 mm^2. It has been difficult to form a plasma jet when the nozzle inner diameter exceeds approximately 10 mm. Here we incorporated a porous ceramic plate perpendicular to the gas flow, which is essential to form a candle-like plasma plume. Hereinafter it is referred to as a plasma candle (patent pending).

2. Experimental

The newly developed plasma candle device consisted of glass tube equipped with porous ceramic plate, ground and high voltage electrodes. Fig. 1 shows (a) the schematic diagram of the plasma candle device (Fig. 1(a)) and the typical shape of the plasma with (Fig. 1(b)) and without (Fig. 1(c)) background air flow for inner diameter of 20 mm, and with background air flow for inner diameter of 31 mm (Fig. 1(d)). In the case of 31 mm (Fig. 1(d)), the plasma candle had less uniformity so the 10 mm and 20 mm nozzles were used in this rest of experiment. The most distinctive character of the nozzle is the presence of a porous ceramic plate being perpendicular to the gas flow. The pore size of the ceramic was found to play a key role in the large sized plasma jet. To study the effect of pore size, five different ceramic plates with pore sizes from 10 μm to 160 μm were tested. These will be referred to based on their mean pore size: CP–13 (10 – 16 μm), CP–28 (16 – 40 μm), CP–70 (40 – 100 μm), and CP–130 (100 –160 μm). The thickness of the porous ceramic plate was constant at 3 mm for all the nozzle sizes. AC high voltage with peak-to-peak voltage of approximately 17 kV_{p-p} with a fixed frequency of 15 kHz was applied to the one of the electrodes. The high voltage electrode was set downstream of the porous ceramic plate. The width of the both high voltage and ground electrodes were fixed at 10 mm.

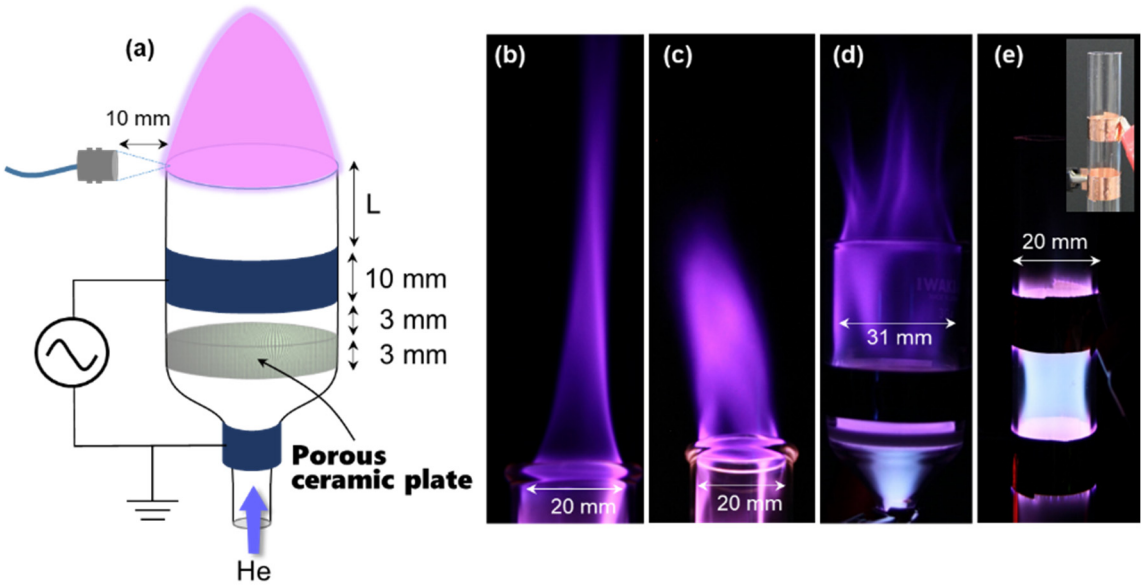

Fig.1. Experimental setup: (a) Schematic of the plasma candle device: (b) plasma shape with i.d. 20 mm, 15.7 kV_{p-p}, and no surrounding airflow near the nozzle: (c) plasma shape with i.d. 20 mm, 15.7 kV_{p-p}, and surrounding air flow (0.3–0.5 m s^{-1}): (d) plasma shape with i.d. 31 mm, 16.5 kV_{p-p}, and no surrounding air flow near the nozzle, and (e) plasma shape without porous ceramic plate with i.d. 20 mm, 17.0 kV_{p-p}. Flow rates of He were 10 L min^{-1} for (b) and (c), and 14 L min^{-1} for (d) and (e). The distances L between the high voltage electrode and the nozzle outlet were 14 mm (i.d. 10 mm), 83 mm (i.d. 20 mm), and 29 mm (i.d. 31 mm).

When the high voltage was connected upstream of the plate, the plasma candle did not appear. Discharge power was measured by the Lissajous figure method [24] using a software (Lissajous Ver 1.72, Insight Co.) [25]. Flow rate of He (99.995% purity) was controlled by a mass flow controller (Kofloc Co, Flow Compo FCC−300) in the range of 1– 14 L min^{-1} (LPM). The plasma candle device and the power supply were installed in a draft chamber. When the induced draft fan of the draft chamber is on, background air flow occurred near the nozzle with a velocity of 0.3 − 0.5 m s^{-1}. As discussed later, the background air flow near the nozzle affected the shapes of plasma candle. Pressure drop in the porous ceramic plate was measured with a digital manometer and was found to vary linearly with the He flow rate. Under typical operating conditions (i.d. 20 mm, He flow rate of 10 L min^{-1}), the pressure drop was observed to be 227.8 Torr (CP–13), 44.8 Torr (CP–28), 19.0 Torr (CP–70), and 4.6 Torr (CP–130), respectively. Owing to the low density of helium (0.138 kg m^{-3}), Reynolds number ($Re = \rho vd/\mu$) is generally low; ρ is the density of gas (kg m^{-3}), v is gas velocity (m s^{-1}), d is the diameter of tube (m), and μ is the dynamic viscosity of gas (Pa·s) . The large diameter of the plasma candle device resulted in a low gas velocity of 0.26 – 0.79 m s^{-1} and, as a result, the Reynolds number was observed in the range 37 – 74 under typical conditions applied in this study.

An intensified charge coupled device (ICCD, Andor iStar DH334T) equipped with a Nikkor UV−105 mm lens was used to capture the plasma jet [26]. A band−pass filter (337 ± 5 nm) was used to monitor the emission of N_2 second positive system ($C^3\prod_u \rightarrow B^3\prod_g$). The ICCD camera was only used for the 10 mm nozzle because the plasma candle with 20 mm diameter exceed the observation area of the ICCD camera. A digital single-reflex camera (Cannon EOS 60D) was also used to record the plasma candle. Gas temperature of the plasma jet was measured using a fiberoptic thermometer (Anritsu, Amoth FX8500). The tip of the sensor was covered with insulator; thus, it could be directly placed in the center of the plasma candle. Temperature resolution was 0.1 °C. The waveforms of applied voltage and discharge current were monitored using a high voltage probe (Tektronix P6015A), a current probe (Pearson current transformer Model 2877 and 101A), and an oscilloscope (Tektronix TDS 3034B). Optical emission spectra between 200 nm and 800 nm was acquired using a spectrometer (Ocean Optics QE65000) and an optical fiber.

3. Results and discussion

3.1 The effect of pore size of ceramic plate on the plasma candle formation

Fig. 2 shows the side view and top view of the plasma for different pore sizes of ceramic plate. Jet formation only occurred with the CP−13 (Fig. 2(a)), which had the smallest pore size. A swirl−like discharge channel on the inner surface of the nozzle seems to be important in forming a jet at the nozzle outlet. The swirl−like pattern was formed at several cm above the ceramic plate. Interestingly, this swirl−like surface stream of plasma did not form for the ceramic plates with larger pore sizes (Fig.2 (b)−(d)). Darny *et al*. reported similar phenomena called helical plasma with an inner diameter of 4 mm tube [27]. Liu *et al*. performed studies on helix plasma in a sealed tube filled with N_2 gas at low pressure (5 kPa) and found that swirling helix plasma stream is forming with or without a helical electrode on the outer surface [28]. Top views of the plasma shape provide an important evidence for why only CP−13 generated a plasma candle. For the other CPs (Figs. 2(b)−2(d)), plasma penetrated the ceramic pores, but not for the CP−13. A similar result has been reported by Hensel *et al* that discharge did not penetrate into porous ceramic when the pore size was smaller than 10 μm [29, 30]. This pore size dependence can be explained by the Paschen's minimum for breakdown. The minimum pressure−gap length product value of He, $(pd)_{min}$, is 2.5 Torr·cm [31]. If we consider pressure drop−corrected pressure, then the minimum gaps for different pores of ceramic plates were as follows: 25.3 μm (CP−13), 31.1 μm (CP−28), 32.1 μm (CP−70), 32.7 μm (CP−130). This estimation clearly indicated that only pore size of the CP−13 was in the left−hand side of minimum gap. When the pore size is smaller than the Paschen's minimum (i.e., for CP−13), it is difficult to form plasma in the inner channels of the porous ceramic; thus, it forms on the surface only. The other three ceramic plates were on the right-hand side of Paschen curve, which may explain why plasma can penetrate through the large pores (CP−28, 70, 130). For the cases of porous ceramic plates of CP−28, 70, and 130, plasma volume is confined between the two electrodes and no plasma surface expansion toward the nozzle outlet was observed. This observation suggested that the CP−13 may separate charges between upstream and downstream of the ceramic plate by preventing plasma penetration through the pores.

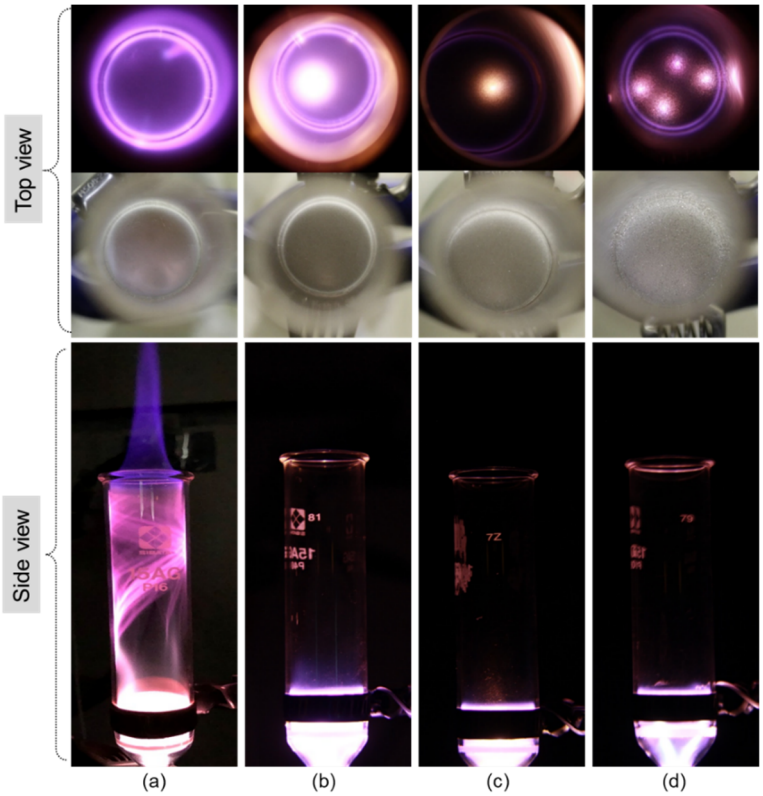

Fig. 2. Top and side views of the plasma candle device with porous ceramic plates with various pore sizes: (a) CP–13 (10–16 μm), (b) CP–28 (16–40 μm), (c) CP–70 (40–100 μm), and (d) CP–130 (100–160 μm). The middle row images present top views of the porous ceramics. Camera exposure time was 0.1 s for (a) and (b), 0.05 s for (c) and 0.01 s for (d). He flow rate and applied voltage were 10 L min^{-1} and 15.6 kV_{p-p}, respectively.

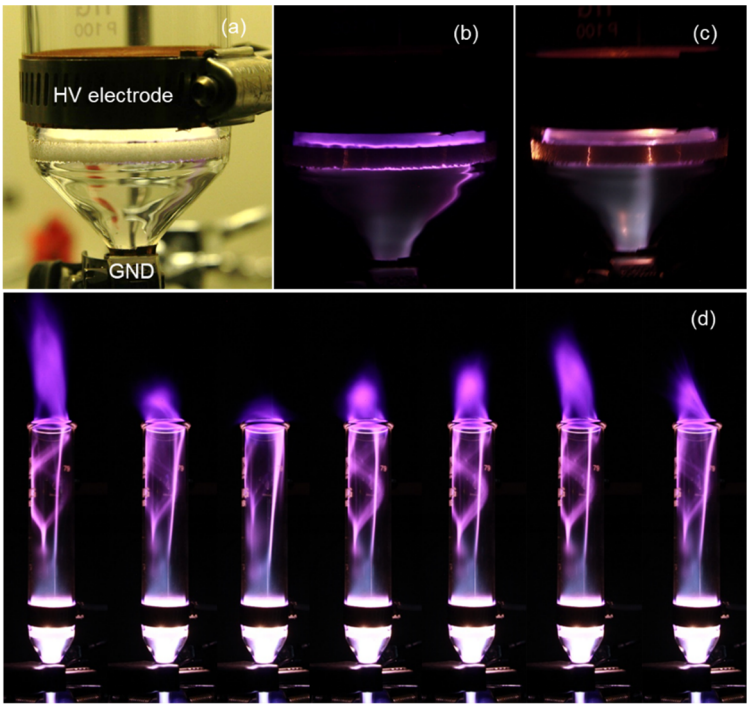

Fig. 3. The shapes of plasma candle; (a) side view of porous ceramic plate, (b) sideview of plasma with the CP–13, (c) sideview of plasma with the CP–70, and (d) sequence photos of plasma candle in the presence air flow near the nozzle (CP–13). Camera exposure time was 1 s for (b) and (c), and 2 s for (d), respectively.

Fig. 3 presents close-up snapshots of plasmas and the influence of background airflow near the nozzle outlet. A porous ceramic plate was placed between the two electrodes. For CP–13 (Fig.3 (b)), plasma was formed at both surfaces of the ceramic plate. This charge separation led to charge build-up and eventually pushed the charges on the inner surface of the nozzle toward the gas outlet. The swirl motion (Fig. 2 (a)) also indicates that plasma extended on the inner surface of the nozzle rather than the volume. In contrast, plasma channels penetrated the ceramic plate in CP–70. As indicated in the experimental section, airflow in the draft chamber affected the shapes of the plasma candle ejected from the nozzle. Fig. 3(d) shows sequence snapshots of plasma candle in the presence of background airflow. Airflow velocity in the draft chamber was comparable with the flow velocity of helium (0.74 m s^{-1} for Fig. 1(b), 0.30 m s^{-1} for Fig. 1(c)), thus rendering the shapes of plasma candle susceptible to the presence of airflow near the nozzle outlet. The long conical shape in Fig. 1(b) disappeared due to the presence of the background airflow. Unless otherwise noticed, the rest of experiments were carried out as the draft chamber remained turned off (i.e., without the background air flow).

3.2 Shape of plasma candle and its characteristics

The characteristics of the plasma candle was further studied using ICCD camera, fiberoptic thermometer, and optical emission spectroscopy. Fig. 4 shows the shape of plasma candle (Fig. 4(b)) and ICCD imaging of the candle (Figs. 4 (c) and (d)) for the 10 mm device. The length of the candle increased with the He flow rate (not shown here). The ICCD images with and without the band-pass filter (337 ± 5 nm) indicated that energy transfer from He* to nitrogen gas molecules occurred near the nozzle outlet and emission of N_2 second positive system ($(C^3\prod_u \rightarrow B^3\prod_g)$ become prominent at the downstream. Fig. 5 indicates the growth pattern of the surface plasma channel with the CP–13 with increasing applied voltage. Near the ignition voltage of 12.1 kV_{p-p}, the plasma region was mostly confined between the electrodes (Fig. 5(b)). At 13.3 kV_{p-p}, as can be seen in Fig. 5(c), the plasma region extended downstream of the high voltage electrode. Two distinctive plasma channels appeared on the inner surface of the tube; one is a linear channel and the other is a swirl-like one. These two channels were reproducible but the swirling pattern seemed to be more important in forming the candle. The starting point of the swirl-like pattern remained constant regardless of applied voltages, but intensity of the swirl increased with the applied voltage. These patterns suggested that a critical charge density is necessary to initiate swirling plasma channel on the inner surface of tube. This observation is consistent with the previous works where the applied voltage (or electric field) plays an important role in the swirling plasma pattern [27, 28]. As can be seen in Fig. 2(a) plasma was separated by the CP–13 plate and charges accumulated on the downstream side of the ceramic plate led the plasma move upward to the tube outlet. This extension of the plasma channel appeared on the inner surface, and eventually formed a jet at the outlet of the nozzle.

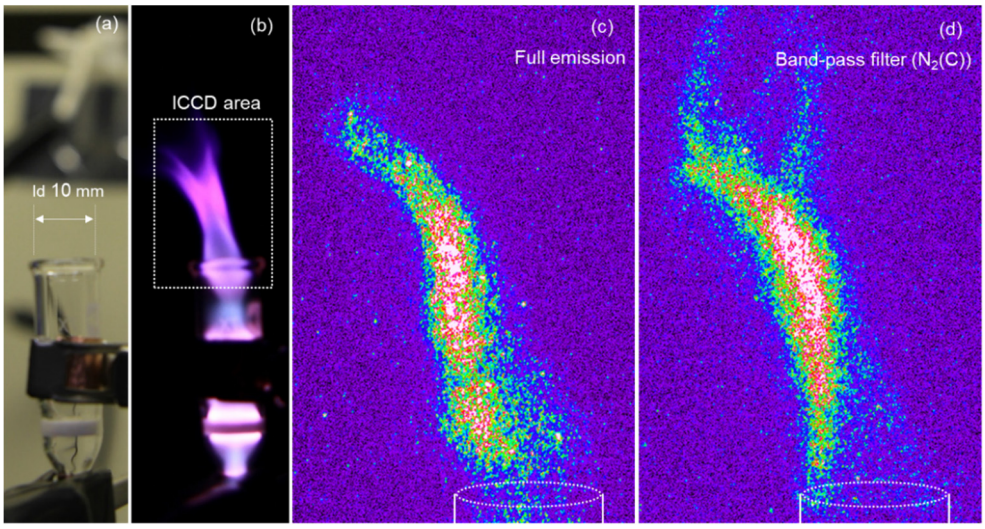

Fig. 4. (a) Photo of i.d. 10 mm nozzle. (b) Shape of the plasma candle for the 10 mm i.d. nozzle (CP–13) with He flow rate of 5 L min^{-1} and applied voltage of 13.7 $kV_{p-p,}$ (c) Single-scan (full emission) ICCD images of the plasma candle. (d) Five-scans accumulated ICCD image of the plasma candle using a band-pass filter (337± 5 nm). ICCD images were taken with 100 μs gage-time.

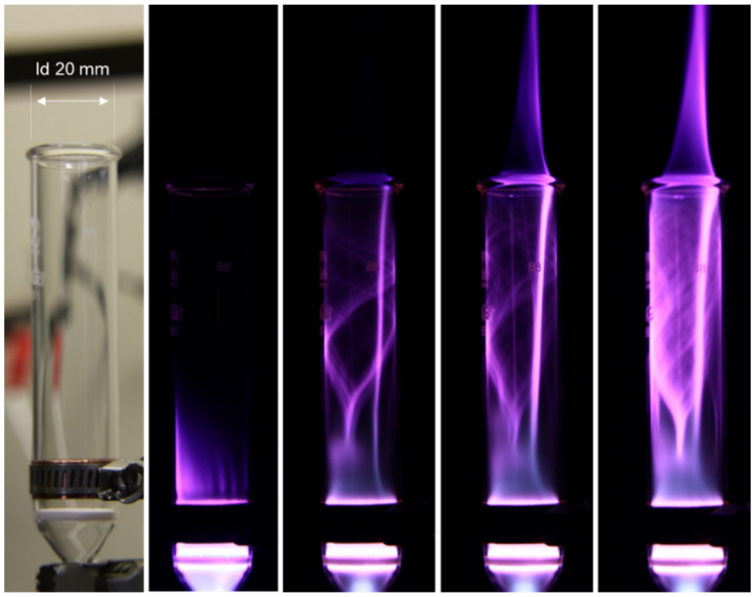

Fig. 5. Extension of plasma channel through the inner surface of the nozzle with the CP–13 (i.d. 20 mm) at applied voltage of (a) 0.0 kV, (b) 12.1 $kV_{p–p}$, (c) 13.3 $kV_{p–p}$, (d) 14.5 $kV_{p–p}$, and (e) 15.7 $kV_{p–p}$.

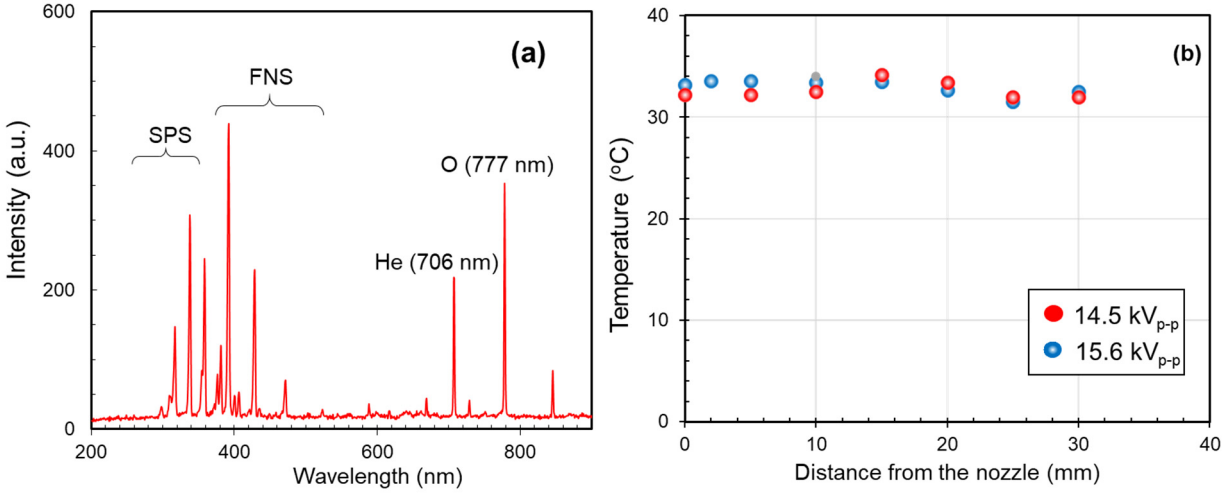

Fig. 6. (a) Optical emission spectroscopy (at 0 mm from the nozzle) and (b) temperature of the plasma candle at different positions and voltage. OES and temperature measurements were done with He flow rate of 10 L min^{-1}. Initial temperature (i.e., plasma off condition) was 25.0 °C.

Fig. 6 shows the optical emission spectrum (a) and temperature (b) of the plasma candle. Optical emission spectroscopy measured at the nozzle outlet revealed that three distinctive groups of emission lines: He, O, and nitrogen species. Both the emission of second positive system (SPS) and first negative system (FNS) were seen at 300 – 400 nm. Atomic oxygen O I lines were found at 777 nm ($3p^5P \rightarrow 3s^5S^0$) and 844 nm ($3p^3P \rightarrow 3s^3S^0$). The strongest line of He was found at 706 nm ($3^3S \rightarrow 2^3P$) and other He lines were appeared at 587 nm, 667 nm and 727 nm. The electric field inside the plasma candle was estimated using the method proposed by Ivkovic *et al* [32], which is based on the intensity ratio of He lines at 667.8 nm and 728.1 nm ($I_{667.8}/I_{728.1}$). The estimated electric field strengths were 8–10 kV cm^{-1} at 11–16 $kV_{p–p}$, which is similar to the values reported by Ivkovic *et al*. The initial gas temperature without plasma was 25.0 °C. The presence of plasma increased the temperature by 7–8 °C in the plasma candle. The temperature at the center of the plasma candle remained constant over the distance up to 30 mm. Applied voltage did not affect the temperature in this study because of the small difference in discharge power between 2.1 W (14.5 $kV_{p–p}$) and 2.5 W (15.7 $kV_{p–p}$).

Fig. 7 shows the effect of He flow rate and applied voltage jet length for 10 mm nozzle (Fig. 7(a)) and 20 mm nozzle (Fig. 7(b)) in the absence of background gas flow near the plasma candle. In the case of nozzle diameter of 10 mm, jet length was highest at 10 kV and decreased with applied voltage. The 20 mm nozzle had longer jet length. These observations are consistent with the results by Li *et al.*, in which the jet length was proportional to the nozzle size [33]. Higher flow rate exhibited a positive influence on jet length for both nozzle sizes, which is identical to the conventional plasma jets with nozzle size below approximately 8 mm [33, 34].

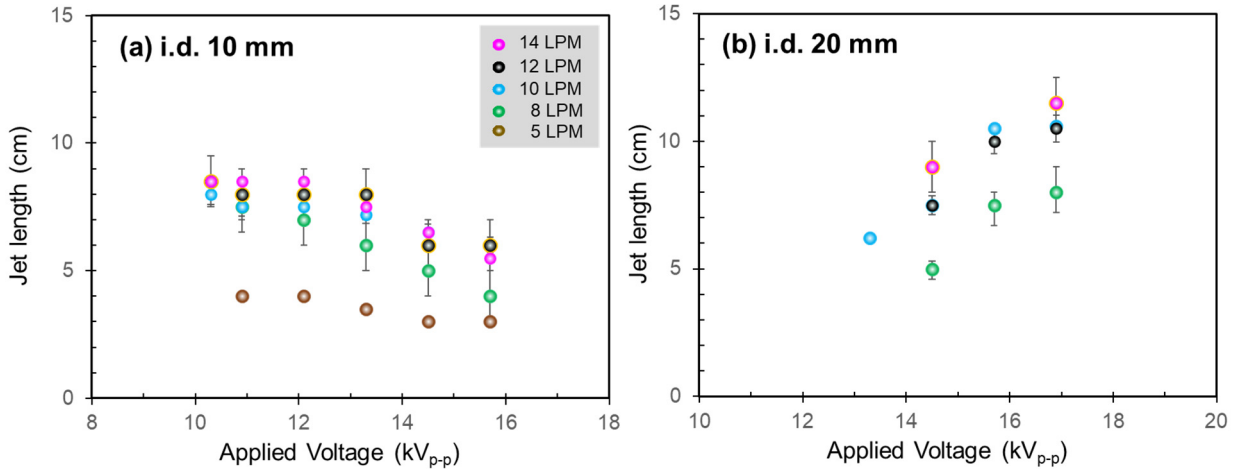

Fig. 7. Effect of applied voltage on jet length for (a) 10 mm nozzle and (b) 20 mm nozzle with the CP−13 plate. The symbols in (a) are the same for the (b).

4. Conclusion

Scale-up of helium plasma jet was achieved by incorporating a porous ceramic plate in the nozzle. Similar to a flickering candle flame, the plasma jet in the new device was susceptible to the surrounding air flow because helium velocity at the nozzle outlet was approximately 0.5 m s^{-1}. This plasma candle can extend the treatment area from ~30 mm^2 using a conventional jet to larger than 314 mm^2. Pore size of the ceramic plates was found to play a key role in forming a plasma candle. When the pore size of the ceramic plate was smaller than the Paschen's minimum, the ceramic plate separated discharge areas above and below the surface of ceramic plate. It was possible to form a stable plasma candle with the inner nozzle diameter of 20 mm. The charge on the downstream side grow on the inner surface of the nozzle as the applied voltage increased and eventually to form plasma candle. The surface evolution of the plasma stream toward the tube outlet is an interesting phenomenon, which however, has an elusive mechanism. The results obtained in this work are preliminary, but nevertheless seem to be very crucial because this new device can extend the jet size beyond the limit of the conventional plasma jets.

Acknowledgment

This work has been supported by JSPS KAKENHI Grant Number JP18H01208.

References

[1] Winter J., Brandenburg R., and Weltmann K. D., Atmospheric pressure plasma jets: an overview of devices and new directions, *Plasma Sources Sci. Technol.*, Vol. 24 (6), pp. 064001, 2015.

[2] Robert E., Sarron V., Ries D., Dozias S., Vandamme M., and Pouvesle J.-M., Characterization of pulsed atmospheric-pressure plasma streams (PAPS) generated by a plasma gun, *Plasma Sources Sci. Technol.*, Vol. 21 (3), pp. 034017, 2012.

[3] Bourdon A., Darny T., Pechereau F., Pouvesle J.-M., Viegas P., Iséni S., and Robert E., Numerical and experimental study of the dynamics of a μs helium plasma gun discharge with various amounts of N_2 admixture, *Plasma Sources Sci. Technol.*, Vol. 25 (3), pp. 035002, 2016.

[4] Laroussi M., Low temperature plasma-based Sterilization: Overview and state-of-the-art, *Plasma Process. Polym*., Vol. 2 (5), pp. 391-400, 2005.
[5] Oh J.-S., Szili E. J., Gaur N., Hong Sung-Ha, Furuta H., Kurita H., Mizuno A., Hatta A., and Short R. D., How to assess the plasma delivery of RONS into tissue fluid and tissue, *J. Phys. D: Appl. Phys*., Vol. 49 (30), pp. 304005, 2016.
[6] Lu X., Keidar M., Laroussi M., Choi E., Szili E. J., and Ostrikov K., Transcutaneous plasma stress: From soft-matter models to living tissues, *Matterials Sci. Eng. R*, Vol. 138, pp. 36-59, 2019.
[7] Bekeschus S., Favia P., Robert E., and Woedtke T.von, White paper on plasma for medicine and hygiene: Future in plasma health sciences, *Plasma Process. Polym*., Vol. 16 (1), e1800033, 2019.
[8] Reuter S., Winter J., Schmidt-Bleker A., Schroeder D., Lange H., Knake N., Gathen V. S.-v. d., and Weltmann K.-D., Atomic oxygen in a cold argon plasma jet: TALIF spectroscopy in ambient air with modelling and measurements of ambient species diffusion, *Plasma Sources Sci. Technol*., Vol. 21 (2), pp. 024005, 2012.
[9] Fujiwara Y., Sakakita H., Yamada H., Yamagishi Y., Itagaki H., Kiyama S., Fujiwara M., Ikehara Y., and Kim J., Observations of multiple stationary striation phenomena in an atmospheric pressure neon plasma jet, *Jpn. J. Appl. Phys*., Vol. 55 (1), pp. 010301, 2016.
[10] Robert E., Sarron V., Darny T., Ries D., Dozias S., Fontane J., Joly L., and Pouvesle J.-M., Rare gas flow structuration in plasma jet experiments, *Plasma Sources Sci. Technol*., Vol. 23 (1), pp. 012003, 2014.
[11] Gherardi M., Puač N., Marić D., Stancampiano A., Malović G., Colombo V., and Petrović Z. L., Practical and theoretical considerations on the use of ICCD imaging for the characterization of non-equilibrium plasmas, *Plasma Sources Sci. Technol.*, Vol. 24 (6), pp. 064004, 2015.
[12] Lu X., Jiang Z., Xiong Q., Tang Z., Hu X., and Pan Y., An 11 cm long atmospheric pressure cold plasma plume for applications of plasma medicine, *Appl. Phys. Lett*, Vol. 92 (8), pp. 081502, 2008.
[13] Jogi I., Talviste R., Raud J., Piip K., and Paris P., The influence of the tube diameter on the properties of an atmospheric pressure He micro-plasma jet, *J. Phys. D: Appl. Phys*., Vol. 47 (41), pp. 415202, 2014.
[14] Topala I. and Nagatsu M., Capillary plasma jet: A low volume plasma source for life science applications, *Appl. Phys. Lett,* Vol. 106 (5), pp. 054105, 2015.
[15] Lacoste D. A., Bourdon A., Kuribara K., Urabe K., Stauss S., and Terashima K., Pure air-plasma bullets propagating inside microcapillaries and in ambient air, *Plasma Sources Sci. Technol*., Vol. 23 (6), pp. 062006, 2014.
[16] Kakei R., Ogino A., Iwata F., and Nagatsu M., Production of ultrafine atmospheric pressure plasma jet with nano-capillary, *Thin Solid Films*, Vol. 518 (13), pp. 3457-3460, 2010.
[17] Nie Q. Y., Cao Z., Ren C. S., Wang D. Z., and Kong M. G., A two-dimensional cold atmospheric plasma jet array for uniform treatment of large-area surfaces for plasma medicine, *New J. Phys.*, Vol. 11 (11), pp. 115015, 2009.
[18] Kim D. Y., Kim J. Y., Chang H., Kim M. S., Leem J.-Y., Ballato J., and Kim S.-O., Low-temperature growth of multiple-stack high density ZnO nanoflowers/nanorods on plastic substrates, *Nanotechnology*, Vol. 23 (48), pp. 485606, 2012.
[19] Cao Z., Walsh J. L., and Kong M. G., Atmospheric plasma jet array in parallel electric and gas flow fields for three-dimensional surface treatment, *Appl. Phys. Lett,* Vol. 94 (2), pp. 021501, 2009.
[20] Kim S. J., Chung T. H., Joh H. M., Cha J.-H., Eom I. S., and Lee H.-J., Characteristics of multiple plasma plumes and formation of bullets in an atmospheric-pressure plasma jet array, *IEEE Trans. Plasma Sci*., Vol. 43 (3), pp. 753-759, 2015.
[21] Robert E., Darny T., Dozias S., Iseni S., and Pouvesle J. M., New insights on the propagation of pulsed atmospheric plasma streams: From single jet to multi jet arrays, *Phys. Plasmas*, Vol. 22 (12), pp. 122007, 2015.
[22] Lietz A. M., Damany X., Robert E., Pouvesle J.-M., and Kushner M. J., Ionization wave propagation in an atmospheric pressure plasma multi-jet, *Plasma Sources Sci. Technol.*, Vol. 28 (12), pp. 125009, 2019.
[23] Dobrynin D., and Fridman A., Planar helium plasma jet: Plasma "bullets" formation, 2D "bullets" concept and imaging, *Plasma Medicine*, Vol. 8(2) pp.177-184, 2018.
[24] Sarani A., Nikiforov A. Y., and Leys C., Atmospheric pressure plasma jet in Ar and Ar/H_2O mixtures: Optical emission spectroscopy and temperature measurements, *Phys. Plasmas*, Vol. 17 (6), pp. 063504, 2010.
[25] Kim H. H., Ogata A., and Futamura S., Effect of different catalysts on the decomposition of VOCs using flow-type plasma-driven catalysis, *IEEE Trans. Plasma Sci*., Vol. 34 (3), pp. 984-995, 2006.
[26] Kim H. H., Teramoto Y., and Ogata A., Time-resolved imaging of positive pulsed corona-induced surface streamers on TiO_2 and γ-Al_2O_3-supported Ag catalysts, *J. Phys. D: Appl. Phys*., Vol. 49 (41), pp. 415204, 2016.
[27] Darny T., Robert E., Dozias S., and Pouvesle J. M., Helical plasma propagation of microsecond plasma gun discharges, *IEEE Trans. Plasma Sci*., Vol. 42 (10), pp. 2506-2507, 2014.
[28] Liu F., Li J., Wu F., Nie L., and Lu X., Effect of external electric field on helix plasma plume, *J. Phys. D: Appl. Phys*., Vol. 51 (29), pp. 294003, 2018.
[29] Hensel K., Katsura S., and Mizuno A., DC microdischarges inside porous ceramics, *IEEE Trans. Plasma Sci.*, Vol. 33 (2), pp. 574-575, 2005.
[30] Hensel K. and Tardiveau P., ICCD camera imaging of discharges in porous ceramics, *IEEE Trans. Plasma Sci*., Vol. 36 (4), pp. 980-981, 2008.

[31] Engel A. v., Ionized Gas. New York: AIP Press, 1993.
[32] Ivkovic S. S., Sretenovic G. B., Obradovic B. M., Cvetanovic N., and Kuraica M. M., On the use of the intensity ratio of He lines for electric field measurements in atmospheric pressure dielectric barrier discharge, *J. Phys. D: Appl. Phys.*, Vol. 47 (5), pp. 055204, 2014.
[33] Li Q., Li J. T., Zhu W. C., Zhu X. M., and Pu Y. K., Effects of gas flow rate on the length of atmospheric pressure nonequilibrium plasma jets, *Appl. Phys. Lett*, Vol. 95 (14), pp. 141502, 2009.
[34] Uchida G., Nakajima A., Takenaka K., Koga K., and Shiratani M., Gas flow rate dependence of the discharge characteristics of a plasma jet impinging onto the liquid surface, *IEEE Trans. Plasma Sci.*, Vol. 43 (12), pp. 4081-4087, 2015.